Protein Science (1993), *2*, 927-935. Cambridge University Press. Printed in the USA.

Molecular dynamics simulations and rigid body (TLS) analysis of aspartate carbamoyltransferase: Evidence for an uncoupled R state

JOHN J. TANNER,[1] PAUL E. SMITH,[1,3] AND KURT L. KRAUSE[1,2]

[1] Department of Biochemistry and Biophysical Sciences, University of Houston, Houston, Texas 77204-5934
[2] Department of Medicine, Baylor College of Medicine, Houston, Texas 77030

(RECEIVED November 9, 1992; REVISED MANUSCRIPT RECEIVED February 19, 1993)

Abstract

In the R form of ATCase complexed with the bisubstrate analogue, *N*-(phosphonacetyl)-L-aspartate, large temperature factors are reported for the allosteric domains of the regulatory chains. We studied the conformational flexibility of the holoenzyme with molecular dynamics simulations and rigid body (TLS) analysis. The results of the molecular dynamics simulations suggest that, although local atomic fluctuations account for the temperature factors of the catalytic and zinc domains, they do not account for the large temperature factors of the allosteric regions. However, the temperature factors of the allosteric domains can be satisfactorily analyzed using a rigid body model. The simulations and rigid body analysis support the idea that the allosteric regions are mechanically uncoupled from the rest of the enzyme in the PALA structure. Implications of this uncoupling for allosteric regulation are discussed.

Keywords: allosterism; aspartate carbamoyltransferase; heterotropic regulation; molecular dynamics; protein dynamics; rigid body motion; TLS

Aspartate carbamoyltransferase (ATCase) has historically been studied as a model for allosteric behavior in enzymes for over three decades (Kantrowitz & Lipscomb, 1990). Although debate exists about which allosteric model is most appropriate for ATCase (Koshland et al., 1966; Schachman, 1988), it conforms to the classical paradigm for allosteric enzymes (Monod et al., 1965) by existing in two main forms (Gerhart & Schachman, 1968), the T state (inactive) and the R state (active). ATCase also demonstrates both homotropic and heterotropic effects (Gerhart & Pardee, 1962; Bethell et al., 1968) involving information flow among the active sites of the catalytic chains in the former and between the regulatory chains and the active sites in the latter. Several high resolution crystal structures of R state, T state, and various intermediate forms have contributed significantly to the understanding of the molecular basis for this regulation (Honzatko et al., 1982; Kim et al., 1987; Krause et al., 1987; Ke et al., 1988; Gouaux & Lipscomb, 1990; Gouaux et al., 1990; Stevens et al., 1990). Complementary information has resulted from biophysical, mutagenesis, and microbiological studies (Kerbiriou & Hervé, 1972; Moody et al., 1979; Wild et al., 1980; Eisenstein et al., 1990; Wild & Wales, 1990; Stevens et al., 1991).

The R state structure of ATCase (Fig. 1) containing the bisubstrate analogue *N*-(phosphonacetyl)-L-aspartate (PALA) was critical in defining the nature of the enzyme's active site and its interactions with substrates, as well as in the delineation of the large structural changes involved in the homotropic allosteric transition (Krause et al., 1987; Ke et al., 1988). One aspect of this high resolution, highly refined crystal structure that has not received extensive comment is the high temperature factors reported for the allosteric regions of the regulatory chains. In the PALA structure the refined *B* factors in these regions average greater than 80 Å^2 and frequently exceed 100 Å^2 (Ke et al., 1988). In contrast, the *B* factors of similar regions in the T state structures are significantly less.

This difference has been attributed to differences in data collection technique (Ke et al., 1988), but the present work suggests that the difference has a physical origin and

Reprint requests to: Kurt L. Krause, Department of Biochemistry and Biophysical Sciences, University of Houston, Houston, Texas 77204-5934.
[3]Present address: Physical Chemistry, ETH-Zentrum, CH-8092, Zurich, Switzerland.

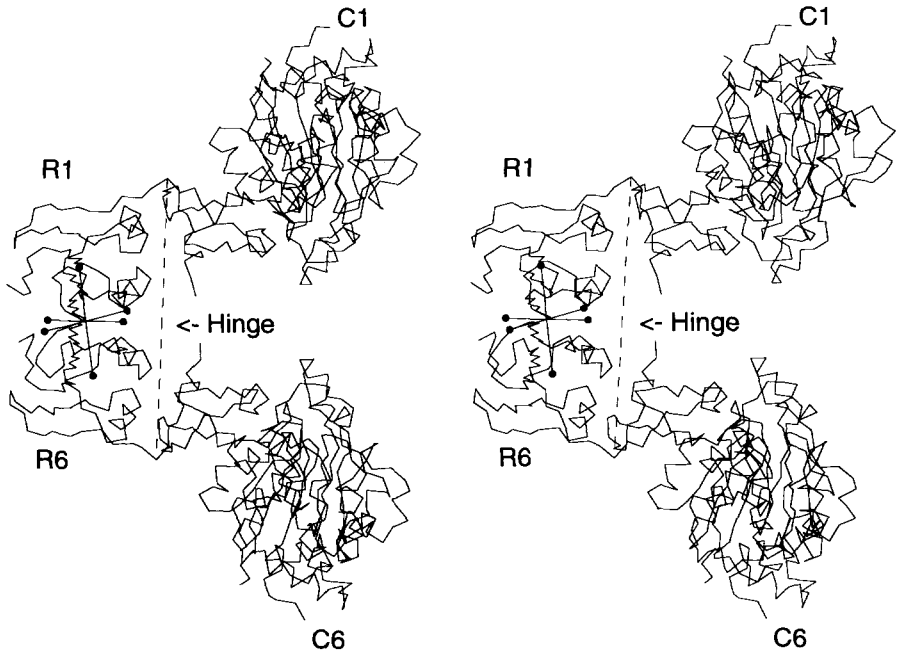

Fig. 1. Stereo view of alpha carbon tracing of the contents of the asymmetric unit of R state ATCase (Ke et al., 1988). There are two catalytic chains, labeled C1 and C6, and two regulatory chains labeled R1 and R6. The three principal libration axes from the TLS fit are pictured at the centroid of the allosteric domains. For clarity, these axes intersect, although in general they need not. A hinge axis, discussed in the Results section, is represented by the dashed line. The dashed line connects residues R1:101 and R6:101. The allosteric domains of the regulatory chains are to the left of the hinge axis, and the zinc domains are to the right of the hinge axis.

functional importance. Although it is tempting to discount these *B* factors as representative of experimental error or a poorly refined structure, several factors weigh against this explanation. First, the native data set was collected using the Xuong/Hamlin area detector system at the University of California, San Diego. It averages five observations per reflection and displays excellent internal R_{sym} values. These data are over 95% complete to 2.5 Å with a substantial number of reflections extending to 2.3 Å. Second, the structure has been refined to an *R* factor of 16.5% while maintaining good geometry. Third, the quality of the electron density in the catalytic chains and the zinc domain of the regulatory chains is excellent. Finally, although the density of the allosteric domain of the R state is difficult to interpret in the N-terminus and the 50's and 90's loops, there is clear but weak density throughout the allosteric region.

Because knowledge of the behavior of the allosteric region of ATCase is important to understanding the basis of its allosteric effects, and because these large temperature factors are unprecedented, we set out to explain their origin. Our hypotheses were that these high *B* factors were due either to large local atomic fluctuations, or that they were due to global, rigid body motion of the allosteric domains relative to the rest of the enzyme. We attempted to deconvolute these two possibilities by performing molecular dynamics (MD) simulations (McCammon & Harvey, 1987; Brooks et al., 1988) of the structure to model the crystallographic temperature factor behavior and rigid body TLS analysis (Schomaker & Trueblood, 1968), which has been shown to model both rigid body motion within proteins and local atomic fluctuations (Sternberg et al., 1979; Kuriyan & Weis, 1991).

We performed simulations of the R state of ATCase in an ideal crystal lattice and also as a holoenzyme. The simulations proved adequate for the catalytic chains and the zinc domain of the regulatory chains in that they returned temperature factors in close agreement to those obtained experimentally. The simulations did not adequately model the experimental results obtained for the allosteric domains. The *B* factors, however, can be fit accurately to a model in which the allosteric domains are considered to be a single rigid body. We suggest that the experimental *B* factors in the allosteric domains reflect large-scale, long time, rigid body motion. In this picture the rigid body motion is a consequence of the uncoupling of the allosteric domains from the zinc domains. Our calculations contribute dynamic evidence, in addition to the known structural evidence (Stevens & Lipscomb, 1992), implicating an uncoupled R state.

Results

Crystal simulation

The root mean square deviation (RMSD) of the alpha carbon backbone from the crystal structure is plotted in Figure 2. The RMSD of the catalytic chains was less than 2 Å, while the RMSD for the regulatory chains was 2.0–2.5 Å. This result was expected because the accuracy of the crystal structure is higher in the catalytic chains than in the regulatory chains (Brooks et al., 1988; Stevens & Lipscomb, 1992). The fluctuations nearly reached their asymptotic values at time = 100 ps, so the *B* factors were calculated from the 100- to 300-ps window of data.

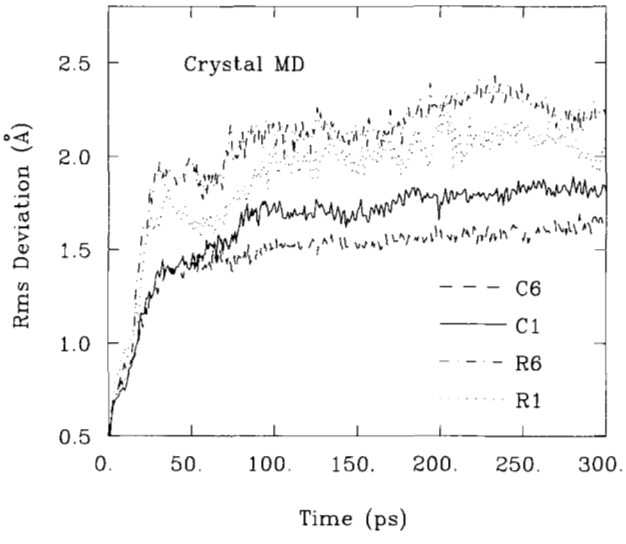

Fig. 2. Root mean square deviation of the alpha carbon backbone of the four polypeptide chains of the asymmetric unit from the crystal structure during the crystal simulation, after least-squares superposition.

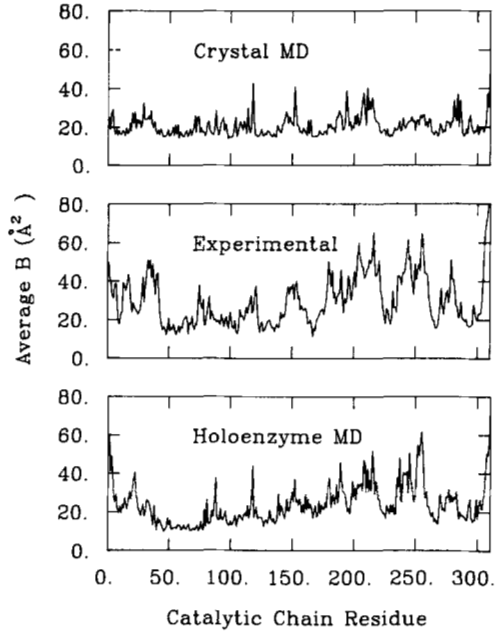

Fig. 3. Average *B* factors for catalytic chain residues obtained from the crystal simulation (top panel), the experimental result of Ke et al. (1988) (middle panel), and the holoenzyme simulation (bottom panel). Data for the two catalytic chains were averaged together. Lattice disorder corrections of 10 Å^2 and 5 Å^2 are included in the *B* factors from the crystal molecular dynamics (MD) and the holoenzyme MD, respectively.

Note that the deviation of C1 differs from that of C6. This result is due to the fact that the two chains have different initial structures, and atoms in the two chains were assigned different initial velocities. Consequently, the two chains explored different regions of phase space. The same argument applies to the regulatory chains. A similar result was observed in a simulation of protease A from *Streptomyces griseus* (Avbelj et al., 1990), in which the time-averaged properties of two identical molecules, which were treated independently, differed. In the present simulation the RMSD between the catalytic chains of the time-averaged structure was 1.8 Å, and the RMSD between the regulatory chains of the time-averaged structure was 2.7 Å.

The experimental and calculated *B* factors are compared in Figure 3 for the catalytic chains and in Figure 4 for the regulatory chains. We augmented the calculated *B* factors with a lattice disorder correction (Northrup et al., 1980) to account for the fact that experimental *B* factors reflect static lattice disorder, in addition to dynamic disorder. Following previous work (Northrup et al., 1980), we assumed that lattice disorder results from translational disorder and derived a correction by requiring that the calculated and experimental *B* factors agree in the protein's interior. The resulting lattice disorder correction was $B_{LD} = 10$ Å^2.

In the catalytic chains (Fig. 3), the qualitative pattern of maxima and minima in the experimental *B* factor profile was captured by the simulation, except near residues 240–260. However, the simulation underestimated the magnitude of some of the maxima in the *B* factor profile. For example, both the calculated and the experimental plots show maxima near residues 35, 215, and 275, but these maxima are more pronounced in the experimental plot.

In the regulatory chains (Fig. 4), the simulation correctly predicted the maxima in the *B* factor profile near regulatory chain residues 37, 53, 65, 90, and 132; however, the simulation underestimated the magnitude of these maxima. Lastly, in the crystal structure, the *B* factors of the allosteric domains (regulatory residues 8–100, also see Fig. 1) are a factor of 1.5–2 larger than those of the rest of the enzyme (Fig. 4, middle panel). In contrast, we found that the fluctuations in the allosteric domains, as predicted by this simulation, were not significantly greater than those in the rest of the enzyme.

Symmetric holoenzyme simulation

The RMSD from the crystal structure (Ke et al., 1988) during the symmetric holoenzyme simulation is plotted in Figure 5. As in the crystal simulation, the catalytic chains were well behaved and had RMSD less than 2.0 Å from the crystal, while the regulatory chains showed a larger deviation. As in the crystal simulation, note that the deviation of C1 differs from that of C6, and that the deviation of R1 differs from that of R6. In particular, regulatory chain R1 had a deviation of 2.7 Å from the crystal structure.

To understand the nature of this motion we independently plot the RMSD of the allosteric and zinc domains

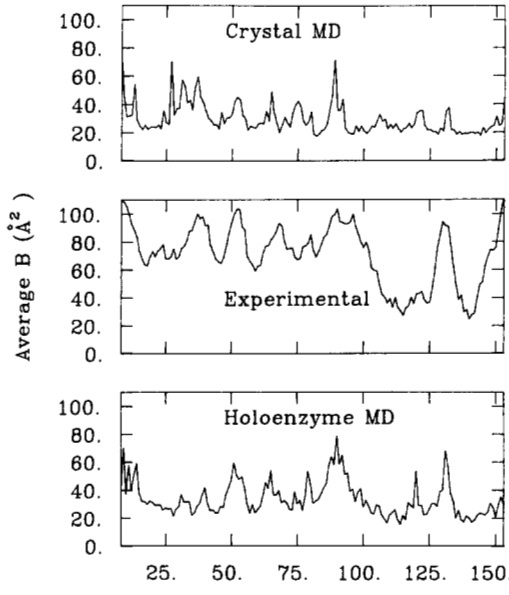

Fig. 4. Average *B* factors for regulatory chain residues obtained from the crystal simulation (top panel), the experimental result of Ke et al. (1988) (middle panel), and the holoenzyme simulation (bottom panel). Data for the two regulatory chains were averaged together. Lattice disorder corrections of 10 Å^2 and 5 Å^2 are included in the *B* factors from the crystal MD and the holoenzyme MD, respectively.

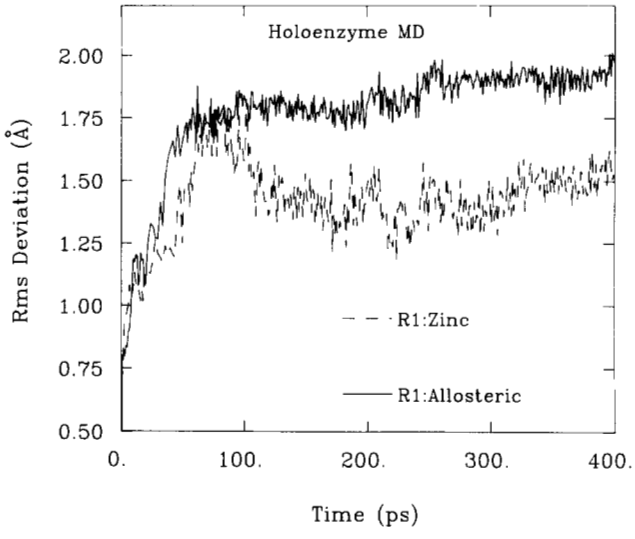

Fig. 6. Root mean square deviation of the domains of regulatory chain R1 from the crystal structure during the holoenzyme simulation, after least-squares superposition. Only alpha carbons were used in the analysis.

of R1 from the crystal structure in Figure 6. The deviations of the domains were below 2 Å, suggesting that their secondary structure was stable, and that the individual domains were stable. Thus, despite the relatively high RMSD of R1, the domains of R1 had low individual RMSD from the crystal structure (Fig. 6), suggesting that relative domain motion occurred. Computer graphics analysis revealed that the allosteric domain of R1 moved slightly toward the zinc domain of R1. This domain motion could be an artifact of the continuum representation of the solvent, and whether it is a feature of the solution structure awaits simulations of solvated models. Despite this domain motion, the RMSD between the regulatory chains of the time-averaged structure was 2.3 Å, which is smaller than the value observed in the crystal simulation. Likewise, the RMSD between the catalytic chains of the time-averaged structure was 1.5 Å, and this value is smaller than we observed in the crystal simulation. Because the domain motion was small, the secondary structure was preserved, and the regulatory chain domains were stable entities, a comparison between the average fluctuations calculated from this simulation with experimental fluctuations is valid.

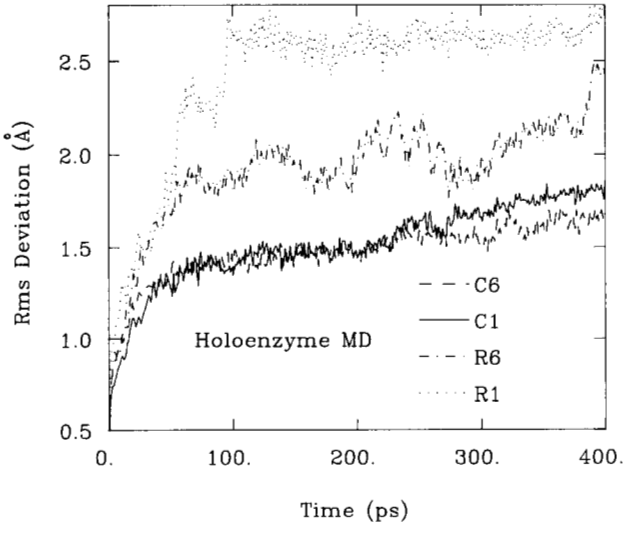

Fig. 5. Root mean square deviation of the alpha carbon backbone of the four polypeptide chains of the asymmetric unit from the crystal structure during the holoenzyme simulation, after least-squares superposition.

The *B* factors calculated from the 100- to 400-ps window of the holoenzyme simulation are plotted in the bottom panels of Figure 3 (catalytic chains) and Figure 4 (regulatory chains). The overall fluctuations in the holoenzyme simulation were larger than those in the crystal simulation, resulting in a lattice disorder correction of 5 Å^2. The agreement between the experimental and calculated *B* factors was better in the holoenzyme simulation than in the crystal simulation. The agreement between experiment and simulation is best in the catalytic chains, where the only area of significant disagreement was a short stretch of residues around residue 33. In the regulatory chains (Fig. 4) we found that the holoenzyme simulation predicted all the major extrema in the experimental *B* factor profile; however, the simulation underestimated the magnitude of the maxima near regulatory chain residue 37, and markedly underestimated the abso-

lute magnitude of the *B* factors throughout the allosteric domains.

The holoenzyme simulation, like the crystal simulation, predicted that the allosteric domains are not significantly more flexible than the rest of the enzyme. If, as suggested by the experimental *B* factors, the allosteric domains are more flexible than the zinc domains and the catalytic chains, then this flexibility does not manifest itself on the time scale of a few hundred picoseconds. An alternate explanation is that the allosteric domains move as rigid bodies on a time scale longer than that of the simulation. To investigate the rigid body nature of the allosteric domains, we fit the experimental fluctuations to the TLS model, which we now discuss.

Rigid body analysis

We performed the TLS analysis using various rigid body definitions, and the results of these calculations are summarized in Table 1. Our goal was to obtain an accurate, physically reasonable fit for all atoms of the asymmetric unit using as few parameters as possible. We began by considering the holoenzyme to be a single rigid body. The resulting TLS fit (entry 1 of Table 1) was reasonable in that the rotational displacements were positive; however, the large RMSD between the observed and TLS *B* factors of 15 Å^2, coupled with the fact that the catalytic chain *B* factors were systematically overestimated and the regulatory chain *B* factors underestimated, prompted us to consider more than one rigid body in our analysis.

We then grouped the four chains of the asymmetric unit together (entry 2, Table 1) but one of the rotational displacements of the resulting fit was negative and exceeded the rejection criterion outlined in the Materials and methods section, so we rejected this scheme. Likewise, if either catalytic chain is grouped with its adjacent regulatory chain, an unphysical fit was obtained (entries 3, 4). We next decomposed the asymmetric unit into four rigid bodies, one for each chain. We obtained good fits for the catalytic chain *B* factors (entries 7, 8), but unphysical negative rotational displacements were obtained in the regulatory chain fits (entries 10, 11). We further decomposed each regulatory chain into two rigid bodies corresponding to the allosteric and zinc domains, but again unphysical rotational eigenvalues were obtained in the fits for both zinc domains (entries 14, 15) and in one of the allosteric domains (entries 12, 13).

Finally, an accurate and physically reasonable fit of all the experimental *B* factors of the asymmetric unit to the TLS model was obtained using the following three-body model. The upper catalytic chain and its adjacent zinc domain formed the first rigid body (C1 + R1:Zinc, entry 5 of Table 1), the lower catalytic chain and its adjacent zinc domain formed the second rigid body (C6 + R6:Zinc, entry 6), and the third rigid body consisted of the two allosteric domains (allosteric dimer, entry 9). We now discuss this three-body fit in detail.

The TLS *B* factors from the three-body model are plotted with the experimental *B* factors in Figure 7. Note that all major features of the *B* factor profiles were reproduced by the TLS model, and in some regions the TLS fit was superimposed on the experimental data. If all the atoms of the asymmetric unit are included, the correlation coefficient, residual, and RMSD between the three-body TLS *B* factors and experimental *B* factors were 0.94, 0.11, and 8.8 Å^2, respectively, indicating that the three-body picture produced the best fit.

Table 1. *Results of TLS analyses*

Fit no.	Rigid body	No. of atoms	CC	R^2	Δ_B (Å^2)	T_{iso} (Å^2)	Rotational displacements $\langle\omega^2\rangle_X$ (deg^2)	$\langle\omega^2\rangle_Y$ (deg^2)	$\langle\omega^2\rangle_Z$ (deg^2)
1.	Holoenzyme	21,270	0.82	0.33	15.1	0.60	0.2	0.2	2.2
2.	C1 + R1 + C6 + R6	7,090	0.85	0.28	14.0	1.12	1.6	−1.1	2.6
3.	C1 + R1	3,545	0.88	0.23	12.4	1.08	4.0	2.8	−1.7
4.	C6 + R6	3,545	0.88	0.22	12.3	1.12	3.1	5.3	−1.5
5.	C1 + R1:Zinc	2,820	0.90	0.19	7.7	0.39	6.8	0.4	2.9
6.	C6 + R6:Zinc	2,820	0.88	0.22	9.1	0.53	6.3	3.6	1.2
7.	C1	2,415	0.86	0.27	6.7	0.38	6.1	3.1	0.1
8.	C6	2,415	0.87	0.24	8.1	0.52	6.2	3.8	1.0
9.	Allosteric dimer	1,450	0.68	0.54	10.0	2.60	1.8	0.5	9.4
10.	R1	1,130	0.83	0.30	11.8	2.54	14.9	−6.0	1.7
11.	R6	1,130	0.87	0.24	10.9	2.46	2.8	17.0	−5.6
12.	R1:Allosteric	725	0.78	0.40	8.2	2.48	8.6	−3.1	13.1
13.	R6:Allosteric	725	0.82	0.34	8.0	2.63	0.8	11.2	6.8
14.	R1:Zinc	405	0.94	0.12	8.0	1.37	9.6	24.7	−2.4
15.	R6:Zinc	405	0.93	0.14	8.7	1.50	28.2	6.9	−3.8

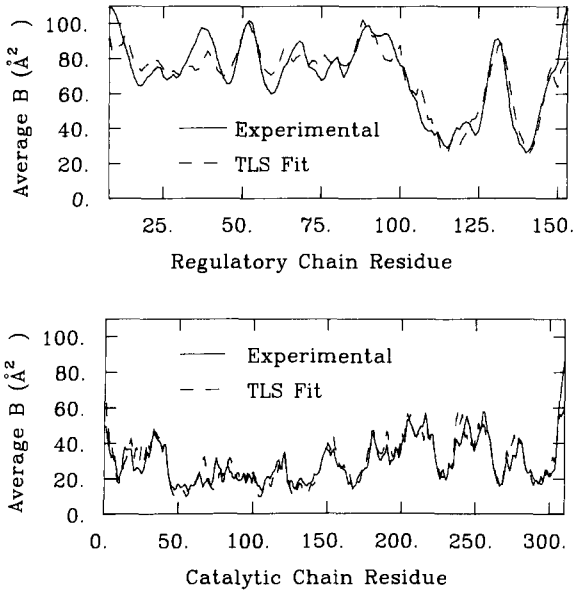

Fig. 7. Comparison of the experimental *B* factors (solid curve, Ke et al., 1988) with the *B* factors from the best fit of the experimental fluctuations to the TLS model (dashed curve). All atoms were used in the fitting procedure, but only the results for the backbone atom are displayed. Results for regulatory chains appear in the top panel (averaged over the two regulatory chains) and results for catalytic chains in the bottom panel (averaged over the two catalytic chains).

The *B* factors in the allosteric domains were accounted for mainly by two components of the TLS model. The largest component was T_{iso}, which contributed 68 Å^2 to the allosteric domain *B* factors (Table 1). Libration was the second largest contribution to the *B* factor, while the screw contributions were relatively small. The principal libration axes of the allosteric dimer are represented (Fig. 1) as three mutually orthogonal axes intersecting at a common origin placed at the centroid of the allosteric dimer. In the case of isotropic *B* factors, the values of T_{iso} and the screw tensor elements are dependent on, but *L* is independent of, the choice of origin. Thus, it is possible to shift the principal libration axes in order to minimize *S* and T_{iso}. Therefore, our picture of the libration axes as mutually intersecting at the centroid is just one representation of the TLS fit.

Note that there is a preferred axis of libration in the allosteric domains, about which the mean rotational displacement is $\langle\omega^2\rangle_Z = 9.4$ deg^2 (Table 1). This axis is nearly vertical in Figure 1. In terms of symmetry axes, the preferred libration axis is approximately orthogonal to the molecular twofold axis that bisects the allosteric dimer of the asymmetric unit, and it makes an angle of about 45° with the crystallographic threefold axis. Finally, the preferred libration axis is closely related (9° offset) to a natural hinge axis of ATCase, namely the axis passing through residues R1:101 and R6:101. The hinge axis is represented by a dashed line in Figure 1, and it makes sense intuitively because it passes through the regions that connect the allosteric domains to the zinc domains.

The success of the three-body TLS fitting, combined with the failure of the simulations to account for the large magnitude of the *B* factors in the allosteric domains, suggests that a model in which the allosteric domains are treated as a single rigid body, loosely coupled to the holoenzyme, could be useful in searching for the causes of these large *B* factors. A more detailed picture awaits further analysis, and it could ultimately involve a combination of hinge bending, static disorder, model error, and experimental error.

Discussion

We performed MD simulations of ATCase in an ideal crystal lattice and as a holoenzyme free of crystal contacts. Both simulations correctly predicted most of the prominent features of the experimental *B* factor profiles, but the level of agreement between simulation and experiment was higher for the holoenzyme simulation. Also, the holoenzyme required a smaller, more reasonable, lattice disorder correction. An important result was that neither simulation predicted the allosteric domains to be more flexible than the rest of the enzyme, which contradicts the level of flexibility implied by the experimental *B* factors. We conclude that the experimental *B* factors of the catalytic chains and the zinc domains of the regulatory chains represent atomic fluctuations occurring on the time scale of a few hundred picoseconds. In contrast, the experimental *B* factors of the allosteric domains are only partially due to such fluctuations.

Upon fitting the experimental fluctuations to the rigid body TLS model, we found that the best fit was obtained when the allosteric domains were considered to be a rigid body. The TLS picture results from a fitting of the full atomic fluctuations as reflected in the temperature factors, thus including both short time and long time fluctuations. The MD results reflect only the short time fluctuations. Comparison of these results suggests that the major contribution to the temperature factors in the allosteric domains arises from global motion (such as hinge bending) that is not apparent at shorter times. This kind of movement of the allosteric domains relative to the holoenzyme suggests that, in the R state, the allosteric domains may act as a single unit, uncoupled from the zinc domains.

Both the simulation and the rigid body analysis support the theory that the allosteric domains are somewhat uncoupled from the enzyme in the R state of ATCase. The structural evidence for an uncoupled R state is that in the T to R transition the distance between the allosteric and zinc domains increases (Stevens & Lipscomb, 1992). We add that a dynamical consequence of this structural change is that the allosteric dimer is free to execute rigid body mo-

tion, such as hinge bending, which results in the experimentally observed flexibility of the allosteric domains.

This picture is appealing in terms of ATCase function because in the R state each of the catalytic chains behaves relatively independently with kinetic profiles approaching a more hyperbolic Michaelis–Menten form. Allosteric domain uncoupling could underlie this shift in kinetic behavior because in the R state the usual pathways for information flow are dramatically altered. For example, no C1–R4 interface exists and the C1–C4 interface is reduced to 240's loop stacking (C4 is related to C6 by threefold symmetry). The only remaining information pathways are within each catalytic trimer and within C1–R1–R6–C6, with the latter often cited as a major conduit of allosteric regulation (Markus et al., 1971; Chan, 1975). Decoupling of the allosteric domains of R1–R6 from the rest of the enzyme would then have the effect of freeing each active site from regulation and allowing the rapid kinetic turnover seen in the R state.

These results may have some implication relevant to the mechanism of the heterotropic allosteric effect in that we can now predict that any effector or mutation that increases the coupling between allosteric and zinc domains will inhibit the enzyme and move it toward the T state, whereas mutations or effectors that decouple the allosteric and zinc domains should increase enzyme activity and promote adoption of the R state.

One recent experimental result can be rationalized on this basis (Van Vliet et al., 1991). In the regulatory chain, Tyr 77 of the allosteric domain is involved in a close contact with Val 106 and Leu 151 of the zinc domain. Tyr 77 was changed to Phe, allowing a tighter association to exist between the allosteric and zinc domains. This mutant enzyme displays predominantly T state characteristics, which is consistent with our analysis. It seems likely that if this hydrophobic interaction is replaced by a salt link, an allosterically locked T form would result.

If correct, the mechanical coupling mechanism provides a basis for explaining heterotropic effects in ATCase, but the molecular details underlying propagation of this effect have been difficult to obtain. Further information about the nature of the rigid body motions in the regulatory chains could be obtained from diffusion models (McCammon & Wolynes, 1977), which have been used to study hinge bending in lysozyme (McCammon et al., 1976), L-arabinose-binding protein (Mao et al., 1982), and antibody molecules (McCammon & Karplus, 1977). We will discuss the application of these diffusion models to the hinge bending of allosteric dimers in a separate communication.

Materials and methods

Crystal structure and nomenclature

The starting structures for the simulations were based on the 2.4-Å resolution crystal structure (R factor = 16.5%) of the enzyme from *Escherichia coli* complexed with the bisubstrate analog *N*-(phosphonacetyl)-L-aspartate (Ke et al., 1988). We obtained atomic coordinates from entry 8ATC of the Protein Data Bank (Bernstein et al., 1977; Abola et al., 1987) at Brookhaven National Laboratory. The hexameric holoenzyme comprises two catalytic trimers and three regulatory dimers, and the unit cell contains two copies of the holoenzyme. The asymmetric unit contains two catalytic chains and two regulatory chains, and the holoenzyme is generated by threefold rotation applied to the contents of the asymmetric unit. The upper catalytic and regulatory chains of the asymmetric unit are related to the lower catalytic and regulatory chains by a noncrystallographic twofold axis, but this constraint was not used in the final crystallographic refinement, thus allowing for differences between the upper and lower chains (Krause et al., 1987; Ke et al., 1988). An alpha carbon trace of the contents of the asymmetric unit is pictured in Figure 1. The two catalytic chains are labeled C1 and C6, and the two regulatory chains are labeled R1 and R6. The allosteric domains of the regulatory chains (residues 8–100) bind nucleotide effectors, and the zinc domains of the regulatory chains (residues 101–153) contain zinc ions, which play a structural role. Each catalytic chain consists of 310 residues and one PALA molecule, and each regulatory chain consists of 146 residues and one zinc ion.

Crystal simulation

We simulated ATCase in an ideal crystal lattice. Thus, only the atoms in the asymmetric unit were explicitly simulated, and the forces due to atoms outside the asymmetric unit were obtained by crystallographic symmetry. Due to computational limitations, inclusion of explicit water molecules was not possible. Therefore, we omitted the 932 crystallographic waters, and used a distance-dependent dielectric constant (Loncharich & Brooks, 1989) to model the solvent. After addition of the polar hydrogens necessary for the CHARMM (Brooks et al., 1983) version 19 united atom force field, the asymmetric unit contained 8,772 atoms.

We combined the CHARMM19 protein and nucleic acid force fields to obtain potential energy parameters for the PALA molecules. The angle-bending and bond-stretching parameters for the extended carbon atom linking the PO_3^{2-} to the carbonyl carbon were obtained by analogy to an ester oxygen. The partial charge of this carbon atom was set to zero.

The zinc ions are tetrahedrally coordinated to the sulfurs of four regulatory chain cysteine residues (Ke et al., 1988). We defined Zn–S bonds, S–Zn–S angles, and Zn–S–C_β angles, and obtained force constants by analogy to parameters used in a simulation of ferrocytochrome c (Northrup et al., 1981). The equilibrium values for the

bond stretching and angle bending of the ZnS_4 complex were obtained from the crystal structure. The force constants were 200 kcal/mol-Å^2 for Zn-S stretching, 5 kcal/mol-rad^2 for S-Zn-S angle bending, and 50 kcal/mol-rad^2 for Zn-S-C_β angle bending. The partial charges for the ZnS_4 fragments were obtained using the electronegativity equalization method (Sanderson, 1983) to distribute the +2 Zn charge partially among the surrounding S atoms. The resulting charges were $Q_S = +0.18$ and $Q_{Zn} = +0.52$. The van der Waals parameters for Zn were $\sigma =$ 1.1 Å, $\varepsilon = 3.125$ cal/mol (Merz, 1991).

We used the program XPLOR version 2.1 (Brünger, 1990) on a Cray Y-MP. The SHAKE algorithm was applied to all bonds, and hydrogens were assigned a mass of 10 amu, allowing a 5-fs time step (Pomes & McCammon, 1990). Nonbonded forces were switched between 6 Å and 7 Å, and the nonbonded cutoff was 8 Å. The nonbonded pair list was updated after an atom moved by 0.5 Å. One picosecond of MD required 20 min of central processing unit time.

We equilibrated as follows. First, we performed 50 cycles of energy minimization. Next, we warmed the system from 0 K to 300 K in steps of 100 K over a 15-ps period, with velocities reassigned to the appropriate Maxwell-Boltzmann distribution every 0.2 ps. Then, we performed 20 ps of MD with coupling to a heat bath at 300 K (atomic friction coefficient = 2 ps^{-1}), followed by 15 ps of MD with velocities reassigned to 300 K every 0.2 ps. During the remaining 250 ps of the simulation, the system was coupled to the 300 K heat bath, and trajectories were written to disk every 0.5 ps.

Symmetric holoenzyme simulation

We also simulated a model of the holoenzyme possessing threefold symmetry, but devoid of crystal contacts. Only the atoms of the asymmetric unit were explicitly simulated, and the forces due to atoms in the other two-thirds of the holoenzyme were obtained by threefold rotational symmetry. One picosecond of simulation required 9 min of Cray Y-MP time. Other details, such as the force field parameters, length of the time step, handling of nonbonded forces, continuum representation of the solvent, etc., were identical to those used in the crystal simulation.

Rigid body TLS analysis

Following previous work (Sternberg et al., 1979; Kuriyan & Weis, 1991), we performed a linear least-squares fit of the experimental atomic fluctuations to the rigid body TLS model (Schomaker & Trueblood, 1968). In this treatment, the mean square displacement of atom i, $\langle \Delta r_i^2 \rangle$, which is related to the isotropic atomic B factor (Willis & Pryor, 1975), $B_i = 8\pi^2 \langle \Delta r_i^2 \rangle / 3$, is expressed as:

$$\begin{aligned}\langle \Delta r_i^2 \rangle = {} & T_{iso} + L_{11}(y_i^2 + z_i^2) + L_{22}(x_i^2 + z_i^2) \\ & + L_{33}(x_i^2 + y_i^2) - 2L_{12}x_i y_i - 2L_{13}x_i z_i \\ & - 2L_{23}y_i z_i + 2S_1 x_i + 2S_2 y_i + 2S_3 z_i. \quad (1)\end{aligned}$$

T_{iso} is the trace of the mean square displacement tensor, $L_{i,j}$ and S_i are tensor elements describing librational and screw motions of the rigid body, and x_i, y_i, z_i are the cartesian coordinates of atom i, relative to the centroid of the rigid body. The mean square displacement is the sum of the mean square displacements along the x, y, and z axes, i.e., $\langle \Delta r^2 \rangle = \langle \Delta x^2 \rangle + \langle \Delta y^2 \rangle + \langle \Delta z^2 \rangle$. All atoms were used in the fitting procedures, but only the results for the backbone atoms are displayed in the results section. The results for side-chain atoms were similar.

The eigenvectors of the libration tensor are the direction cosines of the principal libration axes, and the eigenvalues of the libration tensor are the mean square rotational displacements, $\langle \omega^2 \rangle$, about these axes. Negative libration eigenvalues are unphysical and signal a breakdown of the rigid body model (Kuriyan & Weis, 1991). Following the prescription of Kuriyan and Weis (1991), we rejected a fit if the absolute value of the negative eigenvalue was greater than 10% of the largest positive eigenvalue.

To determine the quality of a given fit we calculated the standard correlation coefficient (CC = 1 corresponds to a perfect fit) and the residual, R^2, defined as:

$$R^2 = \frac{\sum_i [(B_i)_{calc} - (B_i)_{obs}]^2}{\sum_i [B_{mean} - (B_i)_{obs}]^2}, \quad (2)$$

where the summations run over all atoms of the rigid body. The residual indicates the extent to which the model reproduces the deviations of the B factors from the mean, with a value of zero corresponding to perfect agreement (Sternberg et al., 1979). We also calculated the RMSD between the observed and TLS B factors:

$$\Delta_B = \left\{ N^{-1} \sum_i [(B_i)_{calc} - (B_i)_{obs}]^2 \right\}^{1/2}, \quad (3)$$

where N is the number of atoms in the rigid body of interest.

Acknowledgments

This work was supported by a grant from the state of Texas to K.L.K. (ARP3652-245). We acknowledge J. Andrew McCammon for helpful discussions and the San Diego Supercomputing Center for a grant of Cray Y-MP time to J. Andrew McCammon.

References

Abola, E.E., Bernstein, F.C., Bryant, S.H., Koetzle, T.F., & Weng, J. (1987). Protein Data Bank. In *Crystallographic Databases—Information Content, Software Systems, Scientific Applications* (Allen,

F.H., Bergerhoff, G., & Sievers, R., Eds.), pp. 107–132. Data Commission of the International Union of Crystallography, Bonn/Cambridge/Chester.

Avbelj, F., Moult, J., Kitson, D.H., James, M.N.G., & Hagler, A.T. (1990). Molecular dynamics study of the structure and dynamics of a protein molecule in a crystalline ionic environment, *Streptomyces griseus* protease A. *Biochemistry 29*, 8658–8676.

Bernstein, F.C., Koetzle, T.F., Williams, G.J.B., Meyer, E.F., Jr., Brice, M.D., Rodgers, J.R., Kennard, O., Shimanouchi, T., & Tasumi, M. (1977). The Protein Data Bank: A computer-based archival file for macromolecular structures. *J. Mol. Biol. 112*, 535–542.

Bethell, M.R., Smith, K.E., White, J.S., & Jones, M.E. (1968). Carbamyl phosphate: An allosteric substrate for aspartate transcarbamylase of *Escherichia coli*. *Proc. Natl. Acad. Sci. USA 60*, 1442–1449.

Brooks, B.R., Bruccoleri, R.E., Olafson, B.D., States, D.J., Swaminathan, S., & Karplus, M. (1983). CHARMM: A program for macromolecular energy, minimization, and dynamics calculations. *J. Comput. Chem. 4*, 187–217.

Brooks, C.L., Karplus, M., & Pettitt, B.M. (1988). Proteins: A theoretical perspective of dynamics, structure & thermodynamics. *Adv. Chem. Phys. 71*, 1–259.

Brünger, A.T. (1990). *X-PLOR Manual, Version 2.1*. Yale University, New Haven, Connecticut.

Chan, W.W.-C. (1975). Subunit interactions in aspartate transcarbamylase. A model for the allosteric mechanism. *J. Biol. Chem. 250*, 668–674.

Eisenstein, E., Markby, D.W., & Schachman, H.K. (1990). Heterotropic effectors promote a global conformational change in aspartate transcarbamoylase. *Biochemistry 29*, 3724–3731.

Gerhart, J.C. & Pardee, A.B. (1962). The enzymology of control by feedback inhibition. *J. Biol. Chem. 237*, 891–896.

Gerhart, J.C. & Schachman, H.K. (1968). Allosteric interactions in aspartate transcarbamylase. II. Evidence for different conformational states of the protein in the presence and absence of specific ligands. *Biochemistry 7*, 538–552.

Gouaux, J.E. & Lipscomb, W.N. (1990). Crystal structures of phosphonoacetamide ligated T and phosphonoacetamide and malonate ligated R states of aspartate carbamoyltransferase at 2.8 Å resolution and neutral pH. *Biochemistry 29*, 389–402.

Gouaux, J.E., Stevens, R.C., & Lipscomb, W.N. (1990). Crystal structures of aspartate carbamoyltransferase ligated with phosphonoacetamide, malonate, and CTP or ATP at 2.8 Å resolution and neutral pH. *Biochemistry 29*, 7702–7715.

Honzatko, R.B., Crawford, J.L., Monaco, H.L., Ladner, J.E., Edwards, B.F.P., Evans, D.R., Warren, S.G., Wiley, D.C., Ladner, R.C., & Lipscomb, W.N. (1982). Crystal and molecular structures of native and CTP-ligated aspartate carbamoyltransferase from *Escherichia coli*. *J. Mol. Biol. 160*, 219–263.

Kantrowitz, E.R. & Lipscomb, W.N. (1990). *Escherichia coli* aspartate transcarbamoylase: The molecular basis for a concerted allosteric transition. *Trends Biochem. Sci. 15*, 53–59.

Ke, H., Lipscomb, W.N., Cho, Y., & Honzatko, R.B. (1988). Complex of *N*-(phosphonacetyl)-L-aspartate with aspartate carbamoyltransferase. X-ray refinement, analysis of conformational changes and catalytic and allosteric mechanisms. *J. Mol. Biol. 204*, 725–747.

Kerbiriou, D. & Hervé, G. (1972). Biosynthesis of an aspartate transcarbamylase lacking co-operative interactions. I. Disconnection of the homotropic and heterotropic interactions under the influence of 2-thiouracil. *J. Mol. Biol. 64*, 379–392.

Kim, K.H., Pan, Z., Honzatko, R.B., Ke, H., & Lipscomb, W.N. (1987). Structural asymmetry in the CTP-ligated form of aspartate carbamoyltransferase from *Escherichia coli*. *J. Mol. Biol. 196*, 853–875.

Koshland, D.E., Jr., Nemethy, G., & Filmer, D. (1966). Comparison of experimental binding data and theoretical models in proteins containing subunits. *Biochemistry 5*, 365–385.

Krause, K.L., Volz, K.W., & Lipscomb, W.N. (1987). 2.5 Å structure of aspartate carbamoyltransferase complexed with the bisubstrate analog *N*-(phosphonacetyl)-L-aspartate. *J. Mol. Biol. 193*, 527–553.

Kuriyan, J. & Weis, W.I. (1991). Rigid protein motion as a model for crystallographic temperature factors. *Proc. Natl. Acad. Sci. USA 88*, 2773–2777.

Loncharich, R.J. & Brooks, B.R. (1989). The effects of truncating long-range forces on protein dynamics. *Proteins Struct. Funct. Genet. 6*, 32–45.

Markus, G., McClintock, D.K., & Bussel, J.B. (1971). Conformational changes in aspartate transcarbamylase. III. A functional model for allosteric behavior. *J. Biol. Chem. 246*, 762–771.

Mao, B., Pear, M.R., McCammon, J.A., & Quiocho, F.A. (1982). Hinge-bending in L-arabinose-binding protein. *J. Biol. Chem. 257*, 1131–1133.

McCammon, J.A., Gelin, B.R., & Karplus, M. (1976). The hinge-bending mode in lysozyme. *Nature 262*, 325–326.

McCammon, J.A. & Harvey, S.C. (1987). *Dynamics of Proteins & Nucleic Acids*. Cambridge University Press, Cambridge, UK.

McCammon, J.A. & Karplus, M. (1977). Internal motions of antibody molecules. *Nature 268*, 765–766.

McCammon, J.A. & Wolynes, P.G. (1977). Nonsteady hydrodynamics of biopolymer motions. *J. Chem. Phys. 66*, 1452–1456.

Merz, K. (1991). CO_2 binding to human carbonic anhydrase II. *J. Am. Chem. Soc. 113*, 406–411.

Monod, J., Wyman, J., & Changeux, J.-P. (1965). On the nature of allosteric transitions: A plausible model. *J. Mol. Biol. 12*, 88–118.

Moody, M.F., Vachette, P., & Foote, A.M. (1979). Changes in the X-ray solution scattering of aspartate transcarbamylase following the allosteric transition. *J. Mol. Biol. 133*, 517–523.

Northrup, S.H., Pear, M.R., McCammon, J.A., Karplus, J.A., & Takano, T. (1980). Internal mobility of ferrocytochrome *c*. *Nature 287*, 659–660.

Northrup, S.H., Pear, M.R., Morgan, J.D., McCammon, J.A., & Karplus, J.A. (1981). Molecular dynamics of ferrocytochrome *c*. Magnitude and anisotropy of atomic displacements. *J. Mol. Biol. 153*, 1087–1109.

Pomes, R. & McCammon, J.A. (1990). Mass and step length optimization for the calculation of equilibrium properties by molecular dynamics simulation. *Chem. Phys. Lett. 166*, 425–428.

Sanderson, R.T. (1983). *Polar Covalence*. Academic Press, New York.

Schachman, H.K. (1988). Can a simple model account for the allosteric transition of aspartate transcarbamoylase? *J. Biol. Chem. 263*, 18583–18586.

Schomaker, V. & Trueblood, K.N. (1968). On the rigid-body motion of molecules in crystals. *Acta Crystallogr. B24*, 63–76.

Sternberg, M.J.E., Grace, D.E.P., & Phillips, D.C. (1979). Dynamic information from protein crystallography. An analysis of temperature factors from refinement of the hen egg-white lysozyme structure. *J. Mol. Biol. 130*, 231–253.

Stevens, R.C., Chook, Y.M., Cho, C.Y., Lipscomb, W.N., & Kantrowitz, E.R. (1991). *Escherichia coli* aspartate carbamoyltransferase: The probing of crystal structure analysis via site-specific mutagenesis. *Protein Eng. 4*, 391–408.

Stevens, R.C., Gouaux, J.E., & Lipscomb, W.N. (1990). Structural consequences of effector binding to the T state of aspartate carbamoyltransferase: Crystal structures of the unligated and ATP- and CTP-complexed enzymes at 2.6 Å resolution. *Biochemistry 29*, 7691–7701.

Stevens, R.C. & Lipscomb, W.N. (1992). A molecular mechanism for the pyrimidine and purine nucleotide control of aspartate transcarbamoylase. *Proc. Natl. Acad. Sci. USA 89*, 5281–5285.

Van Vliet, F., Xi, X.-G., De Staercke, C., De Wannemaeker, B., Jacobs, A., Cherfils, J., Ladjimi, M.M., Hervé, G., & Cunin, R. (1991). Heterotropic interactions in aspartate transcarbamoylase: Turning allosteric ATP activation into inhibition as a consequence of a single tyrosine to phenylalanine mutation. *Proc. Natl. Acad. Sci. USA 88*, 9180–9183.

Wild, J.R., Foltermann, K.F., & O'Donovan, G.A. (1980). Regulatory divergence of aspartate transcarbamoylases within the enterobacteriaceae. *Arch. Biochem. Biophys. 201*, 506–517.

Wild, J.R. & Wales, M.E. (1990). Molecular evolution and genetic engineering of protein domains involving aspartate transcarbamoylase. *Annu. Rev. Microbiol. 44*, 93–118.

Willis, B.T.M. & Pryor, A.W. (1975). *Thermal Vibrations in Crystallography*. Cambridge University Press, Cambridge, UK.